On the hydrodynamics of membrane assisted fluidized bed reactors using X-ray analysis

Helmi, A.; Wagner, E. C.; Gallucci, F.; Van Sint Annaland, Martin; van Ommen, J. R.; Mudde, R. F.

DOI
10.1016/j.cep.2017.05.006

Publication date
2017

Document Version
Final published version

Published in
Chemical Engineering and Processing: process intensification

Chemical Engineering & Processing: Process Intensification 122 (2017) 508–522

Contents lists available at ScienceDirect

Chemical Engineering & Processing: Process Intensification

journal homepage: www.elsevier.com/locate/cep

On the hydrodynamics of membrane assisted fluidized bed reactors using X-ray analysis

A. Helmi[a], E.C. Wagner[b], F. Gallucci[a], M. van Sint Annaland[a,*], J.R. van Ommen[b], R.F. Mudde[b]

[a] Chemical Process Intensification, Department of Chemical Engineering and Chemistry, Eindhoven University of Technology, P. O. Box 513, 5612 AZ, Eindhoven, The Netherlands

[b] Department of Chemical Engineering, Applied Sciences, Delft University of Technology, van der Maasweg 9, 2629HZ Delft, The Netherlands

ARTICLE INFO

Keywords:
X-ray
Fluidized bed
Vertical membranes
Solids concentration

ABSTRACT

The application of membrane assisted fluidized bed reactors for distributed energy production has generated considerable research interest during the past few years. It is widely accepted that, due to better heat and mass transfer characteristics inside fluidized bed reactors, the reactor efficiency can outperform other reactor configurations such as packed bed units. Although many experimental studies have been performed to demonstrate and monitor the long term performance of membrane assisted fluidized bed reactors, the hydrodynamics of membrane-assisted fluidized bed reactors has thus far only been studied in pseudo-2D geometries. In this work the solids concentration inside a real 3D fluidized bed reactor geometry was measured using a fast X-ray analysis technique. Experiments were conducted in absence and presence of two different membrane modules with different configurations and number of membranes (porous Al_2O_3 tubes) for two types of particles, viz. 400–600 μm polystyrene (Geldart B type) and 80–200 μm Al_2O_3 (Geldart A/B type). Results from the experiments with Geldart B type particles revealed that the membrane modules (both the membranes and the spacers) can significantly reduce bubble growth along the fluidized bed resulting in a smaller average bubble diameter, expected to improve the bubble-to-emulsion mass transfer, whereas for the experiments with fine Geldart A/B particles, and at a very high extraction values (40% of the inlet flow), a densified layer with high solids concentration was formed near the membrane, which may impose an additional mass transfer resistance for gas components to reach the surface of the membranes (concentration polarization). The results from this study help designing and optimizing the positioning of the membranes and membrane spacers for optimal performance of fluidized bed membrane reactors.

1. Introduction

The application of membrane assisted fluidized bed reactors for distributed power production has attracted quite some research interest over the last few years [1]. In a membrane assisted reactor, reaction and separation steps are integrated in one single unit and a high degree of process intensification can be achieved, thereby strongly reducing the required reactor volume and increasing the energy efficiency of the process [2]. It is widely accepted that fluidized bed membrane reactors can outperform packed bed membrane reactor configurations due to their better mass and heat transfer properties [3]. Most of the literature on this topic has been devoted to provide a proof-of-concept at lab-scale or to monitor the long term performance of the membranes at different operating conditions and fluidization velocities [4].

On the material part, the main research effort has been put on the fabrication of membranes with lower price and better permeation properties, i.e. increased permeability and perm-selectivity [3,5–9], whereas for the efficient demonstration of such units it is essential to understand and quantify the reactor design and scale-up parameters that account for the presence of membranes with different permeation values. De Jong et al. performed an extensive study on the hydrodynamics of fluidized beds in the presence of horizontally integrated membranes inside a pseudo 2D fluidized bed [10]. For this study a combined particle image velocimetry and digital image analysis (PIV/DIA) technique was used. The experimental results confirmed that for the membrane assisted bed the average equivalent bubble diameter was decreased by a factor of about 3 in comparison with the case where no membrane was integrated due to the increased bubble break-up (while the average bubble size was hardly affected by the permeation ratio through the membranes). In another study it was confirmed that the presence of horizontal membranes in the bed decreases the average bubble size, but the formation of gas pockets around the tubes need to

* Corresponding author.
E-mail address: m.v.sintannaland@tue.nl (M. van Sint Annaland).

http://dx.doi.org/10.1016/j.cep.2017.05.006
Received 29 December 2016; Received in revised form 5 May 2017; Accepted 8 May 2017
Available online 17 May 2017
0255-2701/

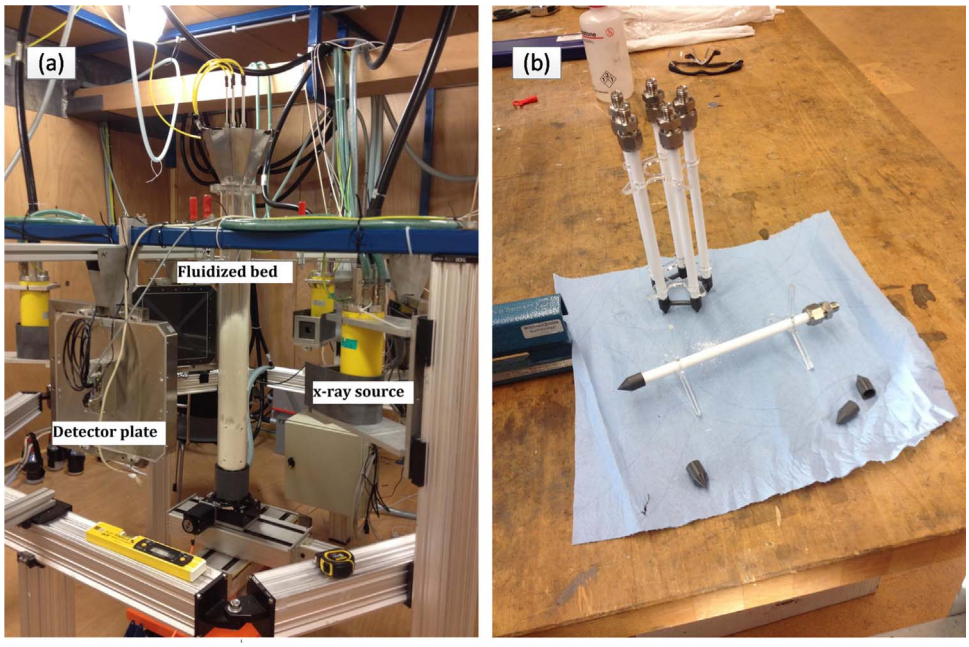

Fig. 1. (a) The designed fluidized bed placed between the X-ray source and the detector plate (b) Membrane modules of one and five membranes with spacer plates and sealing.

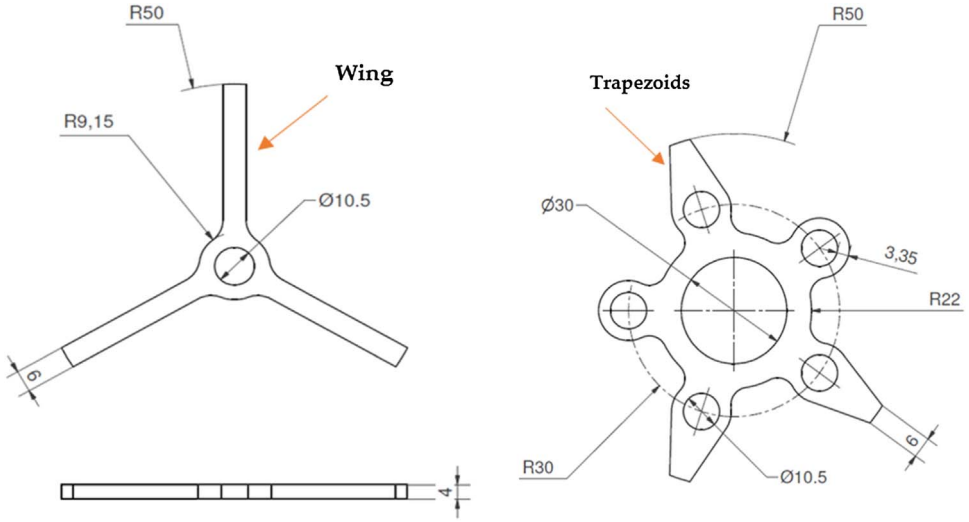

Fig. 2. Spacer plates (left) spacer designed for the membrane module with one single membrane in the middle of the reactor and (right) spacer plate designed for the membrane module with five membranes in a star shape configuration (all measures are in mm).

Table 1
Relative area of the spacers to the reactor cross sectional area.

Module	Number of membranes	Spacer section area 10^{-4} m^2	Reactor cross section area 10^{-4} m^2	Spacer area/ Reactor cross section area (%)
I	1	9.12	78.5	11.6
II	5	19.8	78.5	25.2

Table 2
Physical properties of the used particles.

Material	Avg. particle diameter[a] [μm]	Apparent Density (g/cc)[b]	Minimum fluidization velocity[c](U_{mf}) [cm/s]	Geldart classification [23] [–]
Polystyrene	500	1.06*	22.0	B
Al_2O_3	160	1.691	2.4	A/B

[a] FRITSCH ANALYSETTE22.
[b] ThermoFisher SCIENTIFIC Pascal 140 series.
[c] By measuring the pressure drop over the distributor plate and the bed.
* From [19].

be properly accounted for when determining the average bubble size to avoid underestimation, while these gas pockets may also decrease the performance of the membrane reactor [11].

Dang et al. [12] and De Jong et al. [10] experimentally studied the solids circulation patterns in pseudo 2D fluidized beds (from relatively large beds to micro-structured beds) with gas extraction via membranes (filters) installed in the walls of the reactor also applying the combined PIV/DIA technique. It was found that in the cases where a large amount of gas is extracted via the membranes, the solids concentration in the near vicinity of the membrane increases and may result in the formation of so-called densified zones, which may impose an additional mass transfer resistance for gas components to reach the surface of the membranes. These findings are in accordance with a discrete particle simulation study done by Tan et al. [13]. These results have also been

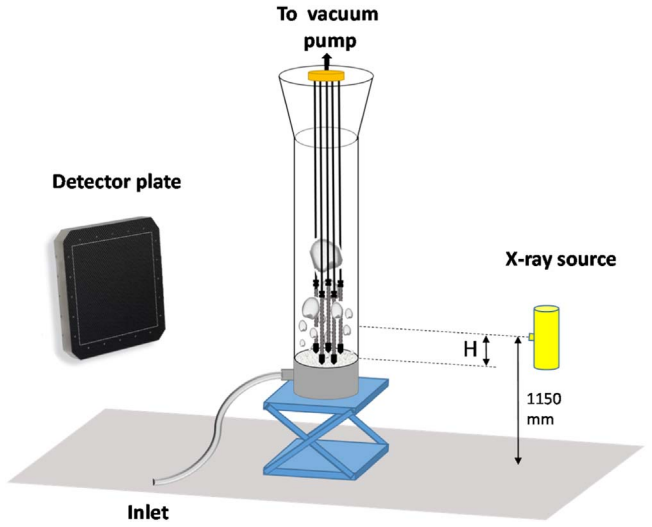

Fig. 3. A schematic representation of the experimental setup with the reactor in the center of the setup. The reactor was scanned at four different axial positions H (mm):0, 80, 160 and 240 mm.

confirmed in case membranes (filters) are installed at the back plate of the pseudo 2D reactor [14].

Although these studies all point towards the possibility of the formation of densified zones close to the membrane surface thereby inducing external mass transfer limitations that can limit the performance of fluidized bed membrane reactors, an extension of the study to 3D fluidized beds in the presence of and with permeation through vertically immersed membranes is required for a better understanding and improved design of membrane assisted fluidized bed reactors. Unfortunately, the technique used so far (PIV/DIA) is restricted to 2D geometries only, as it requires visual access to the reactor.

Recently, a detailed study was devoted on the effect of vertically immersed internals on the performance of a lab-scale and a pilot-scale fluidized bed heat exchanger in a real 3D reactor geometry utilizing an ultra-fast X-ray tomography technique [15–17]. It was generally found that the immersion of internals results in a lower average bubble size along the fluidized bed.

In the present work the hydrodynamics of a fluidized bed reactor will be investigated in the presence of vertically immersed porous membranes in a real 3D reactor geometry using a fast X-ray analysis technique. With the help of this technique the hydrodynamics of the fluidized bed membrane reactor is monitored with very high spatial and temporal resolution. The paper is outlined as follows: first the materials, set-up, the technique and data processing methods used in this study will be described in detail. Subsequently, the obtained results for different operating conditions will be presented and discussed, followed by a summary of the main conclusions.

2. Materials and methods

2.1. Experimental

In this study the solids concentration inside the fluidized bed was measured using the fast X-ray analysis technique developed by Mudde et al. [18]. The setup originally consisted of three standard industrial type X-ray sources (Yxlon International GmbH) with a maximum energy of 150 keV working in fan beam mode. Detailed information on the specification of the X-ray sources can be found elsewhere [19]. Each X-ray source generates a fan beam that can be detected by a detector plate on the opposite side of each X-ray source. For this study the experiments were performed with one X-ray source and one detector plate to obtain the projected 2D output signals from the 3D bed.

For the experiments a lab scale fluidized bed reactor was placed (inclination ± 2 mm/m) in the center of the setup and 1140 mm from the X-ray source and 501 mm from the detector plate. For each experimental condition the attenuation of the X-ray beam was measured with a frequency of 35 Hz at the detector plate purchased from Teledyne Dalsa Inc (Xineos-3131® 30 × 30 cm in size). The theoretical spatial resolution of the detector is 0.2 mm per pixel. The measured data at the detector plate were stored on a PC for further analysis.

The entire experimental procedure was controlled with a workstation outside the setup room (covered with a lead sheet) ensuring a safe working condition. Using the workstation it was possible to trigger the X-ray source and read out the signals from the detector plate. Further details on the setup and the measurement technique can be found in [15,16,18]. Each result reported in the present study is an average of 2100 frames (at 35 Hz) of one minute of continuous recording from one source and one detector plate. The sampling time of one minute allows to obtain sufficient data for statistics with a minimum error from the mean [15].

The lab-scale fluidized bed reactor was constructed of Perspex® and 10 cm in inner diameter (5 mm wall thickness) and 100 cm in length. The inlet was connected to compressed air controlled by a Bronkhorst® type mass flow controller. The size of the reactor is similar to the size of small scale fluidized bed reactors for micro heat and power applications

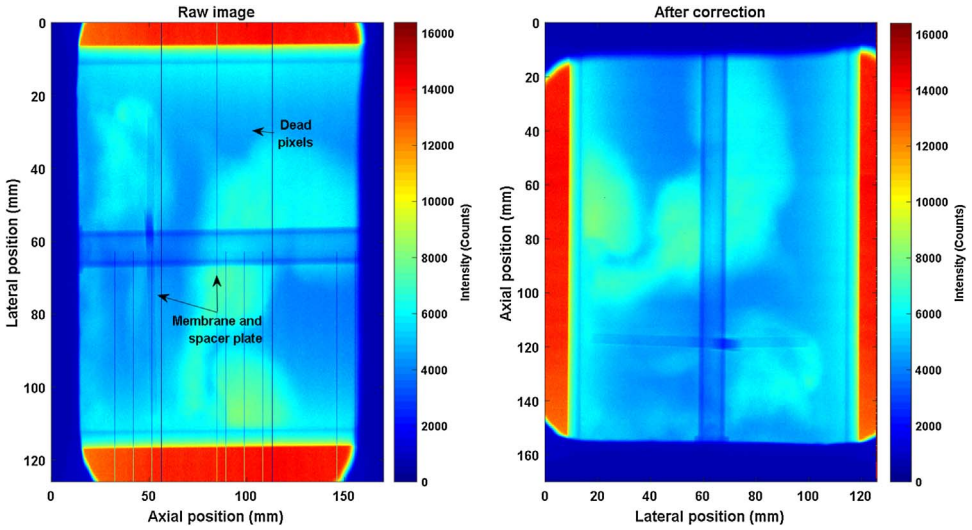

Fig. 4. (left) raw intensity map recorded at the detector plate. Frame needs to be corrected for dead pixels, orientation and contrast (right) dead pixels have been replaced by the average value of the neighboring cells; image has also been corrected for contrast and orientation. Geldart B type particles at U/U_{mf} = 2, H = 80 mm.

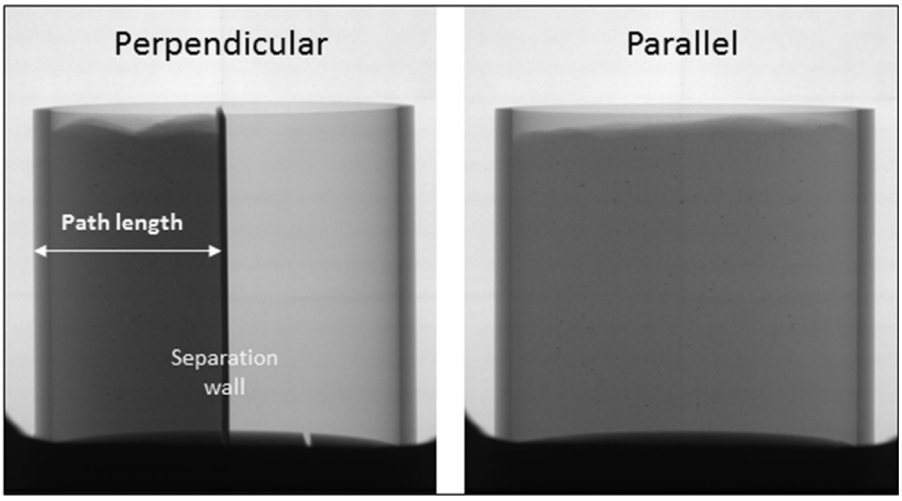

Fig. 5. Calibration module filled 2/4th with polystyrene particles and (a) Separation wall is perpendicular to the X-ray source (b) Separation wall is parallel to the X-ray source.

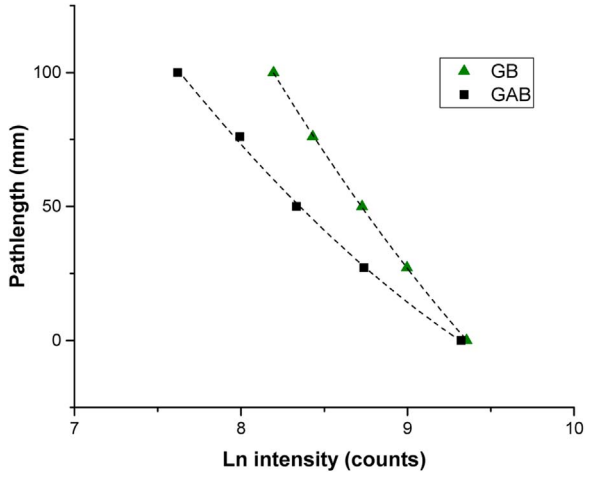

Fig. 6. Fitted calibration curves for different particles. GB: polystyrene and G_{AB}: Al_2O_3 particles.

[20]. The gas distributor plate was made of sintered stainless steel (40 μm pore size, 3.2 mm thick from Van Borselen Filters) to ensure a homogenous distribution of the gas at the bottom of the column. To minimize particle entrainment from the column a freeboard was designed and installed at the top part the reactor. Fig. 1a shows a picture of the fluidized bed column placed between the X-ray source and the detector plate.

The immersed membranes were porous Al_2O_3 (100 nm pore size at the surface). Each membrane was 20 cm in length and 1 cm in outer diameter sealed to a plastic cap from one side and to a stainless steel Swagelok component (with graphite ferrule) from the other side [6]. At the outlet of the column, the membranes were connected to a 12 mm outlet tube that was connected to a vacuum pump (TRIVAC Leybold LH) with a capacity of 40 ln/min of air, which could be controlled with a Brooks® mass flow controller (0–44 ln/min) using Labview software. Due to the pressure drop in the lines from the outlet of the membrane module to the vacuum pump, a total flow rate of 10 ln/min of air could be maximally extracted via each membrane at room temperature and 1 bar pressure difference across the membrane. It should be noted that without the pressure drop in the lines a total flow rate of 22 ln/min could be extracted via each membrane at similar operating conditions [21].

Two different membrane modules were designed: one module with one membrane in the center of the reactor and one module with five membranes in a star configuration. For each membrane module, two spacer plates made from Perspex® were used to keep the membrane(s) in place and avoid any movement during fluidization. Such spacers are generally used when submerging membranes in fluidized bed reactors [20,22]. Fig. 2 shows a schematic representation of the membrane spacers and their specifications. Table 1 summarizes the relative area of the spacers to the reactor cross-sectional area. Although it is important to use spacers to keep the membranes in place and avoid breakage of the membrane tubes, it is expected that the spacer plates may also affect the fluidization due to their presence. Also the influence of the spacers on the hydrodynamics is investigated in this paper.

Two different types of particles were used in this study. The first batch was 400–600 μm polystyrene particles and the second batch was 80–200 μm Al_2O_3 particles. For all the experiments the stagnant bed height of the particles was 30 cm from the distributor plate (bed aspect ratio of 3) to ensure full immersion of the membranes inside the bed at minimum fluidization conditions. Table 2 summarizes the physical properties of the used particles.

To capture the behavior over the full length of the bed, and due to the fact that the detector plate and the X-ray source were fixed in place, the reactor module was relocated vertically using an adjustable table. For each single experiment, measurements were performed four times and at four different distances of the X-ray source from the distributor plate (H value in Fig. 3), allowing to compare the average properties of the bed at vertical positions in the bed for the different cases. Before the recordings were started, the bed was first stabilized for 30 min.

The column was filled with particles and aligned in the middle of the X-ray source and the detector plate. According to the performed

Table 3
Fitting parameters for the calibration curves (y = Intercept + B1*X + B2*X2 and X is the Ln of intensity).

Particle	Intercept		B1		B2		Statistics
Al_2O_3	Value	Standard error	Value	Standard error	Value	Standard error	Adj. R^2
Path length	1292.6	3.05×10^{-12}	−235.5	7.22×10^{-13}	10.38	4.26×10^{-14}	1
Polystyrene	Value	Standard error	Value	Standard error			Adj. R^2
Path length	1827.36	1.04×10^{-11}	−320.1	2.37×10^{-12}	13.34	1.35×10^{-13}	1

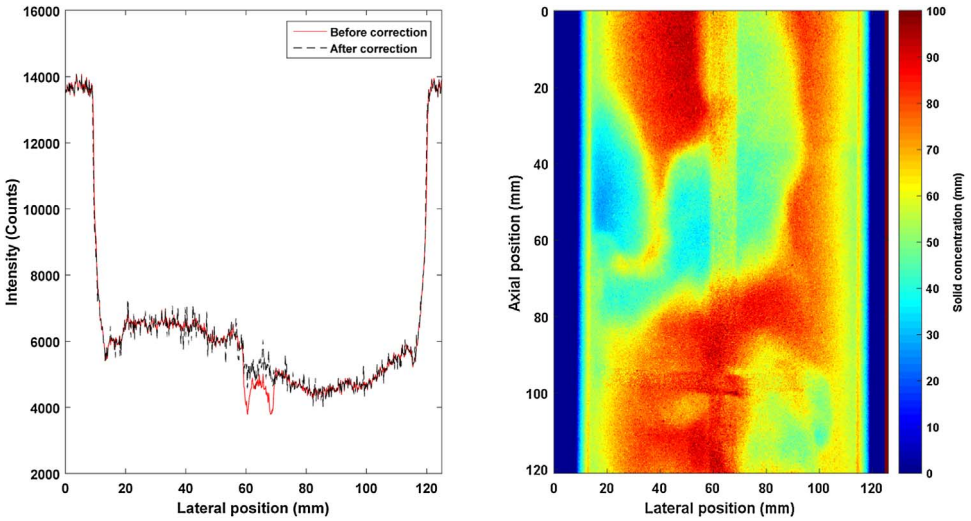

Fig. 7. (left) Output intensity profile at a certain reactor height (70 mm above the distributor plate) across the bed width before and after image correction for the presence of the membrane (right) converted intensity map to solids concentrations (path length); at $U/U_{mf} = 2$ and H = 80 mm.

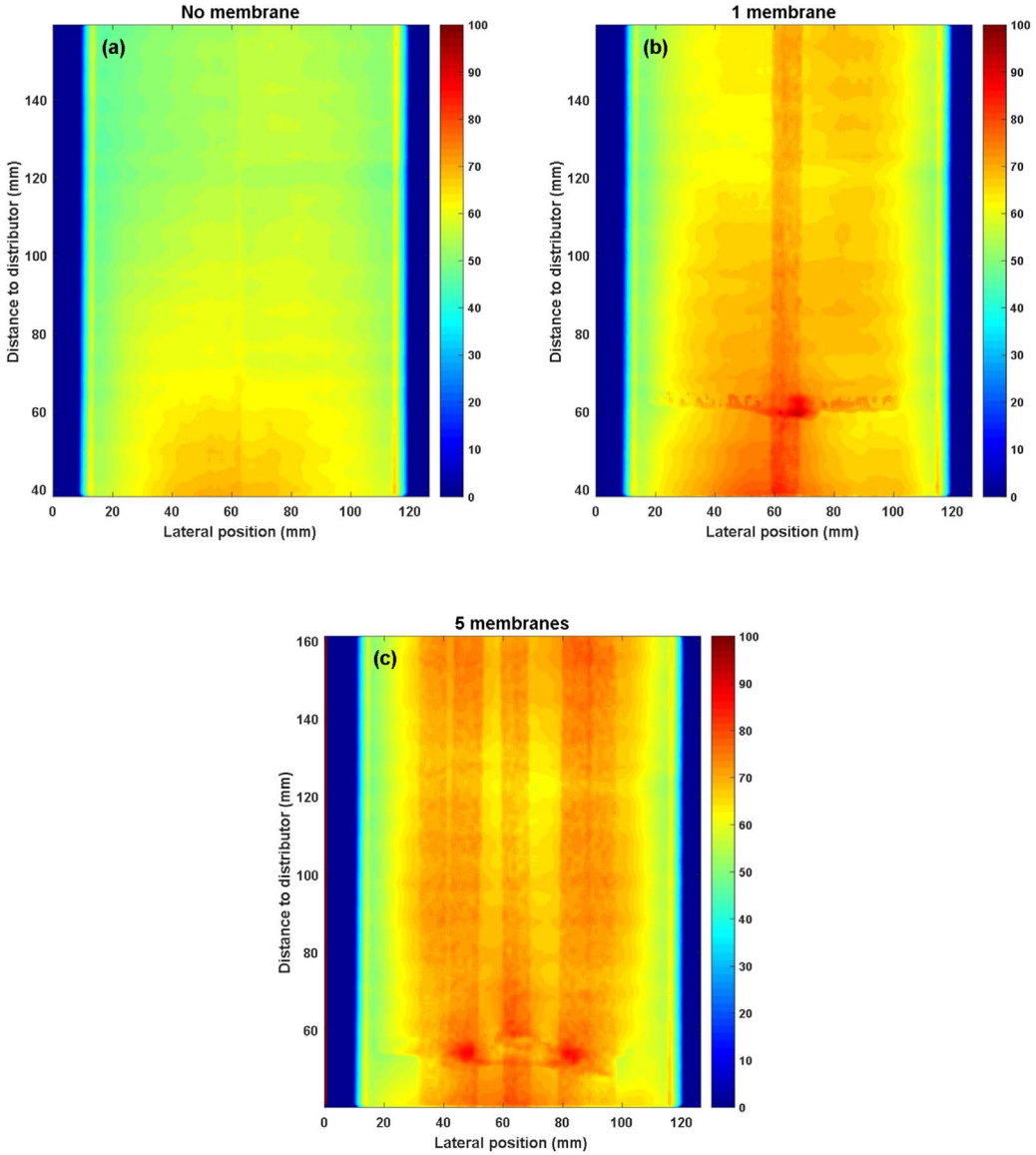

Fig. 8. Time-averaged normalized solids concentration map for three cases: (a) standard fluidized bed without membrane module; (b) Fluidized bed with one single membrane in the middle without gas extraction; (c) Fluidized bed with 5 membranes in a star configuration without gas extraction.

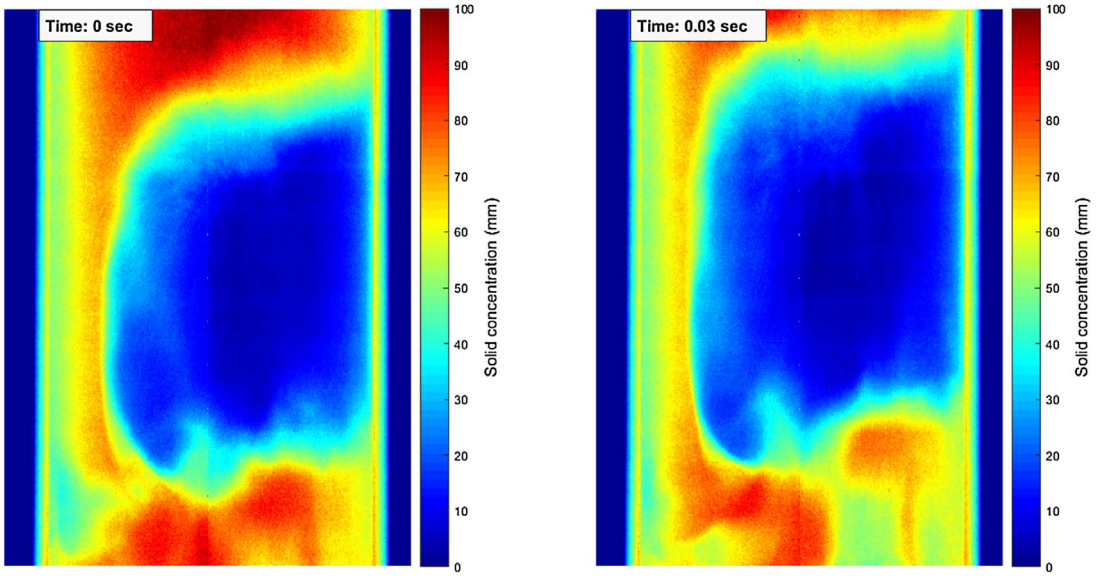

Fig. 9. Snapshots from the experiments without membrane modules; Geldart B (Polystyrene) particles; U/Umf = 2, H = 80 mm.

contrast tests at bubbling fluidization conditions, the X-ray source and camera settings were determined to ensure a very good contrast between the bubble and the emulsion phases. First, experiments were performed without the membrane modules (standard fluidized bed) to monitor the bed behavior at different fluidization numbers (0–3.5) and particle types (both Geldart B and Geldart A/B particles). Subsequently, the membrane modules with one and five membranes were immersed inside the bed and experiments were repeated at identical conditions (compared to the standard fluidized bed) without gas extraction via the membranes to quantify the effects of only the presence of the vertically immersed internals. In the last set of experiments, different amounts of gas (compressed air, up to 40% of the inlet flow rate) was extracted through the membranes and the bed behavior was monitored at otherwise identical operating conditions.

2.2. Image analysis

For each experiment, the attenuation of the X-ray beam was measured for each pixel at the detector plate to have the projected 2D intensity map of the bed in time. For each obtained single frame, initially the image was corrected for dead pixels caused by imperfections of the detector plates: the measured attenuation of each dead pixel was replaced by the mean value of the neighboring cells. Then, the frames were cropped to the desired region of interest for each experiment. To have the actual view of the column each frame was rotated 90° and flipped. Fig. 4 shows the result of the performed image correction protocol for a typical single frame image.

To convert the measured attenuation (intensity) to a solids concentration (path length), a calibration protocol that has already been reported in [16] was performed. A dummy calibration module made of identical material (Perspex®) and with identical inner diameter (100 mm) and wall thickness (5 mm) as the fluidized bed reactor was constructed (Fig. 5). The height of the dummy column was 10 cm.

Initially the dummy module was placed (1140 mm from the X-ray source and 501 mm from the detector plate) and aligned (± 2 mm/m) between the X-ray source and the detector plate. The height of the column was adjusted to ensure that the whole module was covered at the detector plate. Afterward, the module was filled in a segment wise mode (using a separation wall for the different segments) with different amount of particles (polystyrene or Al_2O_3). For each case the attenuation of the outlet X-ray beam from the column was measured at a pixel pocket (50 × 50 px^2) at the detector plate. Fig. 5 shows the dummy module half filled with polystyrene particles when the separation wall was perpendicular and parallel to the X-ray source.

For all the experiments it was ensured that the separation wall (used to fill the column in segments) was parallel to the X-ray source (90° rotation from the case where the separation wall is perpendicular to the X-ray source). Knowing the exact thickness (path length) of the particle slice, the attenuation of the X-ray beam was converted to a path length of material inside the bed. Five different segments (empty bed, 1/4th, 2/4th, 3/4th and full bed) were chosen for the calibration curve.

Fig. 6 shows the fitted (2nd order logarithmic) calibration curves for polystyrene (Geldart B) and Al_2O_3 (Geldart A/B) particles (error is below 3% or 2 mm of bed depth). Detailed information on the fitting parameters can be found in Table 3.

For the experiments using the membrane modules, the intensity maps needed to be corrected for the effect of the membranes on the output intensity. To correct for the presence of the membrane(s) in each frame and for each experiment, two cases with and without membrane presence at $U/U_{mf} = 0$ were selected. Theoretically, if an X-ray beam with initial intensity of I_0 passes through a stagnant bed of particles with a bed thickness of d_p and reactor wall thickness of d_w, the outlet intensity (I) of the beam can be calculated with Eq. (1).

$$I/I_0 = e^{[-\mu_w d_w - \mu_p d_p]} \tag{1}$$

where μ represents the attenuation coefficient of the media (using subscripts w and p to refer to the reactor wall and particle phase, respectively). If a single membrane is submerged in the middle of the bed, for the outlet intensity of the X-ray beam in the presence of the membrane (I′), Eq. (1) can be rewritten as:

$$I'/I_0 = e^{[-\mu_w d_w - \mu_p d_{p'} - \mu_m d_m]} \tag{2}$$

where $d_{p'}$ is the corrected thickness of the bed at the presence of the membrane (d_m is the outer diameter of the membrane):

$$d_{p'} = d_p - d_m \tag{3}$$

so that

$$\alpha = \ln I/I' = d_m(\mu_m - \mu_p) \tag{4}$$

where α represents the net contribution of the membrane presence on the intensity profile. Also where the membrane spacers are located, α will include the effect of spacers as well. For each frame, the α value at each pixel was added to the logarithm of intensity at the corresponding pixel. Later the exponential of the product was calculated to obtain the

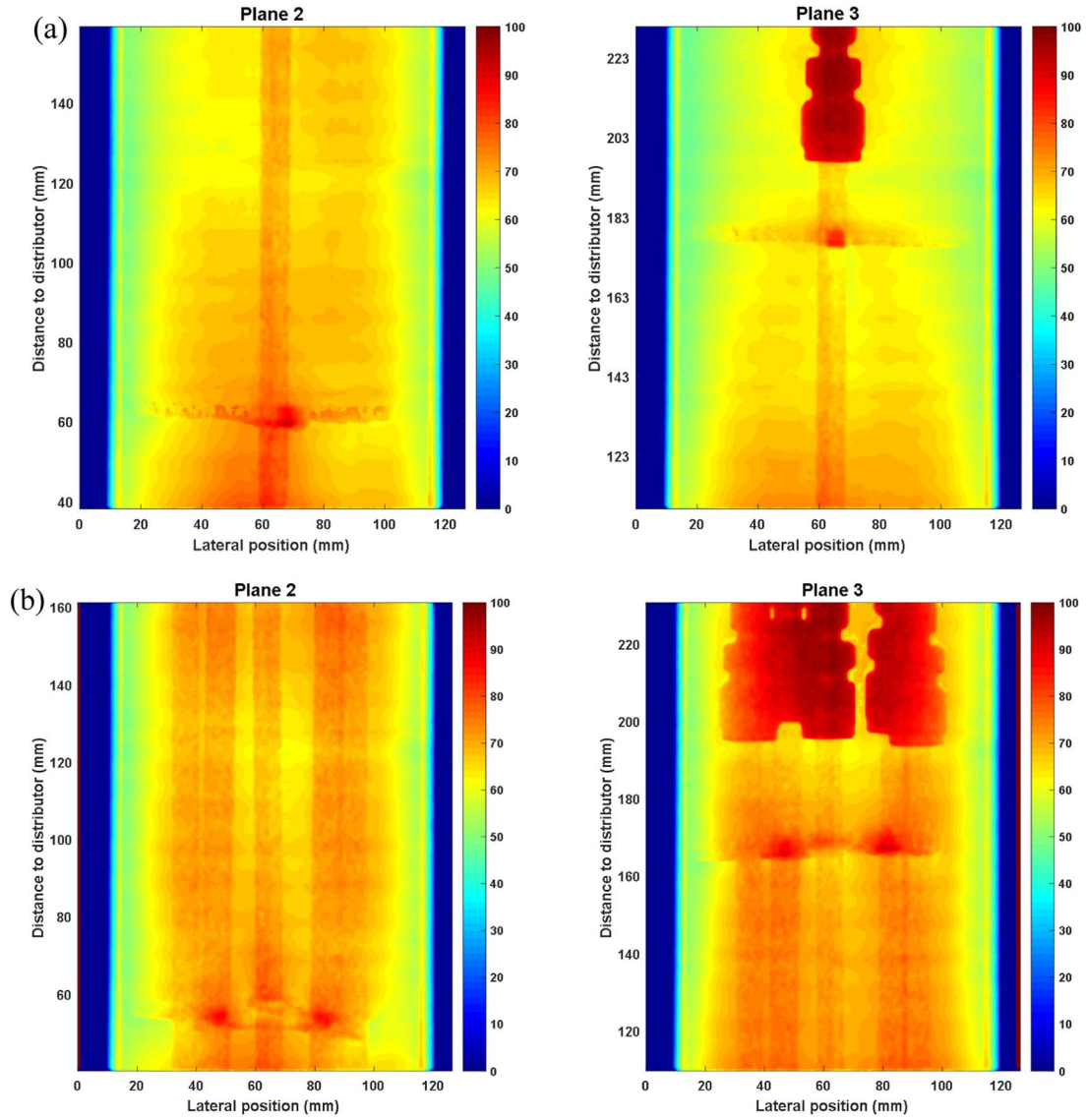

Fig. 10. Average solids concentration maps inside the fluidized bed and along the membrane(s) (a) One single membrane immersed inside the fluidized bed (b) Membrane module with five membranes is immersed; H = 80 mm at plane 2 and H = 160 mm for plane 3, for all the cases the outlet velocity was kept the same at $U/U_{mf} = 2$. The color bars represent the normalized solids concentration in mm of particles path length (zero represents the empty bed and 100 stands for packed bed).

corrected intensity map. Fig. 7 shows the results of the membrane correction and calibration steps for a selected frame.

For each experiment a standard sample of 2100 frames (at 35 fps) equal to 1 min of continuous recording was chosen. Each frame was corrected according to the previously described image correction protocol. In the next section the output results from the experiments will be analyzed and the main conclusions will be drawn accordingly.

3. Results and discussion

The obtained results from the experiments at different operating conditions and membrane reactor configurations will be discussed and analyzed in two parts. In the first part, the average solids concentration maps for the cases with and without membrane presence will be discussed for the polystyrene particles (Geldart B), showing the effect of the different number of inserted membranes and the extent of gas extraction on the average solids concentration maps. Subsequently, the dynamics of the bubble phase along the reactor module will be discussed and recommendations will be given on the design of such membrane reactor units.

The second part of the discussion focuses on the results obtained with alumina particles (Geldart A/B) and the bed behavior in the absence and presence of the membrane modules together with different extraction values. Specifically the average solids concentration fields at different positions in the lateral position of the column (from the membrane surface to the reactor wall) will be inspected to investigate the probability of formation of densified zones, and quantification of their thickness, in the case of very high gas extraction values.

3.1. Geldart B

3.1.1. Effect of internals

First the effect of internals on the hydrodynamics of the fluidized bed filled with polystyrene particles was studied. Three cases were selected: (1) standard fluidized bed without internals, (2) fluidized bed with the membrane module containing one single membrane in the middle of the reactor, but without gas extraction, and (3) fluidized bed with the membrane module with five membranes arranged in a star shape, also without gas extraction. For all these cases the outlet velocity was kept the same, implying that the inlet flow rate was corrected for the presence of the membrane(s). Fig. 8 shows the obtained time-averaged (over 1 min of recording) solids concentration fields (in mm of

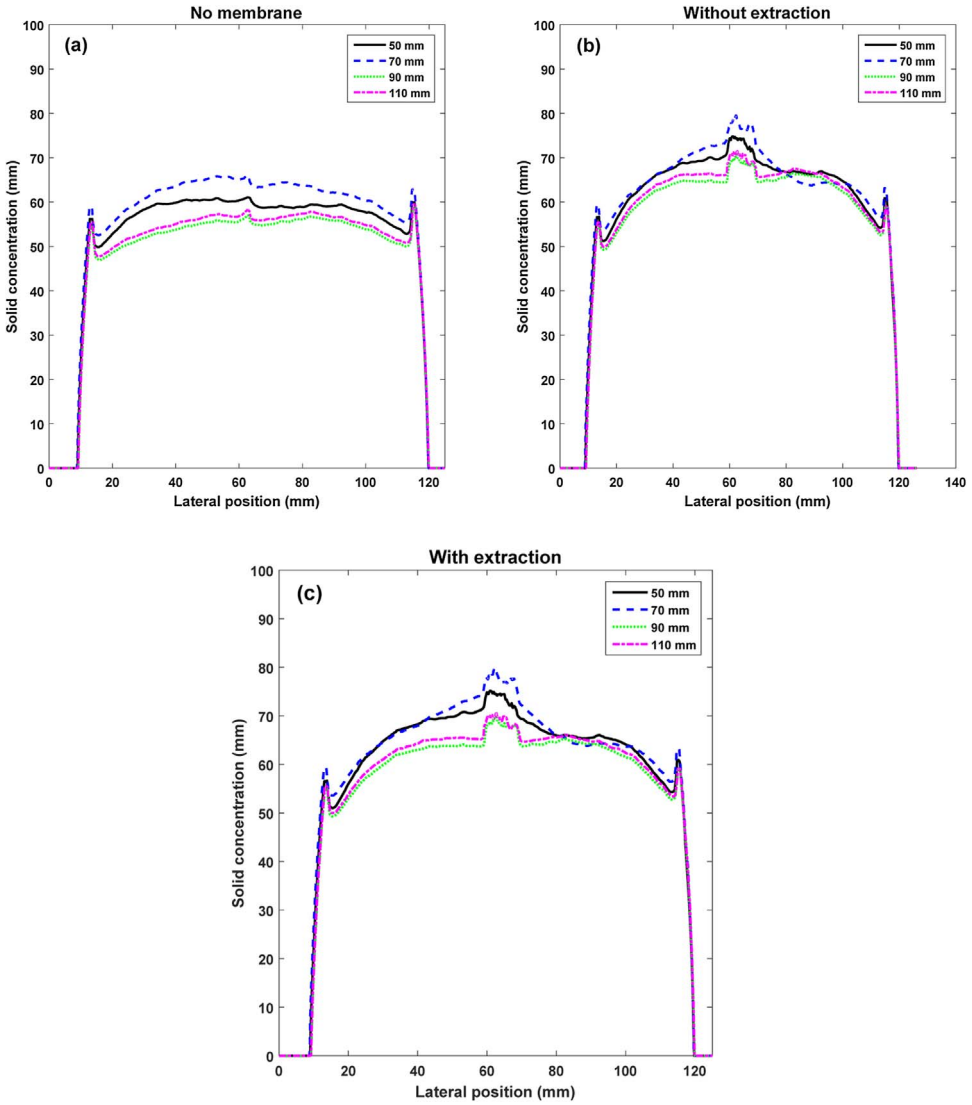

Fig. 11. Time-averaged lateral solids concentration profiles at different heights from the distributor plate: (a) standard fluidized bed without membranes; (b) fluidized bed with one single membrane in the middle without gas extraction; (c) fluidized bed with one single membrane in the middle and 10 ln/min gas extraction. For all the cases the outlet velocity was kept at $U/U_{mf} = 2$.

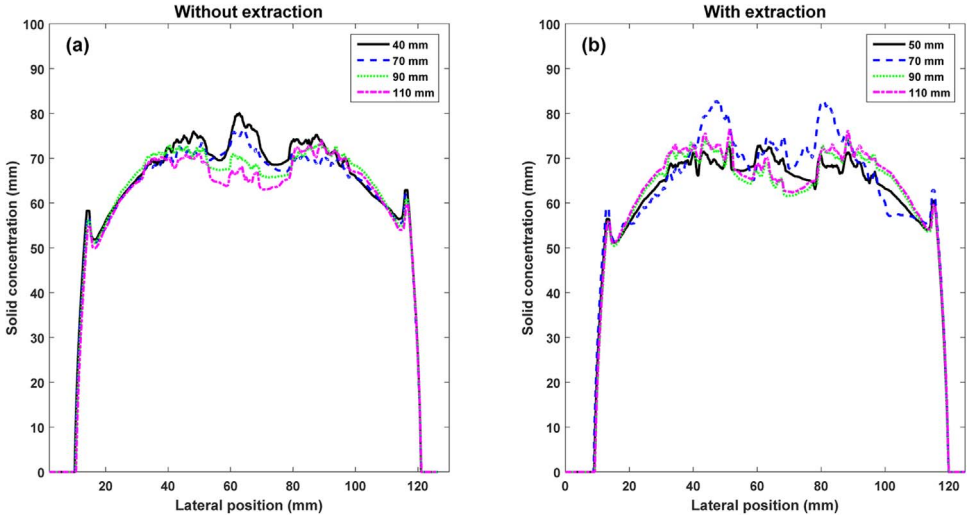

Fig. 12. Time-averaged lateral solids concentration profiles at different heights from the distributor plate: (a) fluidized bed with the membrane module with 5 membranes in a star configuration and without gas extraction; (b) fluidized bed with the membrane module with 5 membranes in star configuration and 25 ln/min gas extraction (12.5% of the inlet flow). For all the cases the outlet velocity was kept at $U/U_{mf} = 2$.

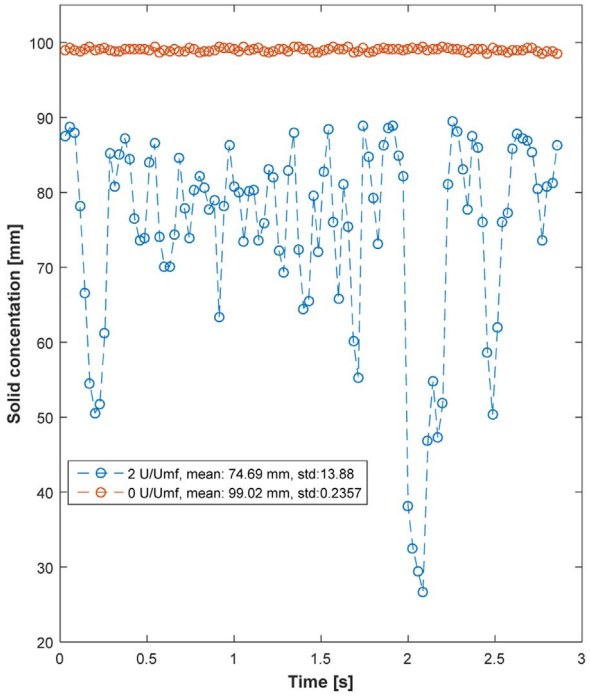

Fig. 13. Output solids concentration signal in time at U/Umf = 0 and U/Umf = 2 (data was collected at 100 mm from the distributor plate and at r/R = 0.5).

solids path length) for the three cases. The color bar represents the normalized solid concentrations (in mm of solids path length), where 100 represents the maximum solids packing of a fixed bed (inner diameter of the reactor is 100 mm) and zero stands for an empty bed.

Fig. 8a shows that for the standard fluidized bed case without immersed membranes the time-averaged normalized solids concentration decreases in the axial direction, as expected, corresponding to the well-known bubble growth and coalescence. However, the measured values of the solids concentration were relatively low. Inspecting the snapshots from the experiments (Fig. 9) heavy slugging of the bed is clearly visible, as may have been expected related to the small bed diameter and relatively large size of the particles. Once the membrane module with one single membrane in the middle of the bed was immersed, the degree of slugging was largely decreased (Fig. 8b). This is attributed to increased bubble break-up because of the presence of the immersed membrane and membrane spacer.

Fig. 8c shows the time-averaged solids concentration for the case with the membrane module consisting of five membranes immersed inside the fluidized bed. In comparison with the case with one single membrane in the middle, the solids concentration is increased along the membrane module and around the membranes. The maximum solids concentration was found at the bottom spacer plate and close to the membranes. It should be noted that for all the cases higher solids concentrations were observed close to the surface of the membrane(s) than in the bulk of the fluidised bed.

3.1.2. *Effect of spacers*

Fig. 10a shows the time-averaged solids concentration field for the case with one single membrane immersed in the middle of the bed at $U/U_{mf} = 2$ for different vertical positions. It can be seen from the results at plane 2 (i.e. at H = 80 mm) that at the bottom of the membrane and close to the bottom spacer the solids concentration is somewhat higher indicating that more gas bubbles move along the reactor walls. Passing over the membrane spacer the gas bubbles tend to travel back to the middle of the reactor where the membrane is. Moving higher in the fluidized bed to plane 3 (H = 160 mm), the average bubble size increases and the average solids concentration decreases. For the single membrane module the effect of the second spacer at the top on the hydrodynamics is much less pronounced in comparison to the effects of the bottom spacer. This may imply that there is an optimum distance between the spacers for maximum bubble cutting.

When the membrane module with five membranes was immersed

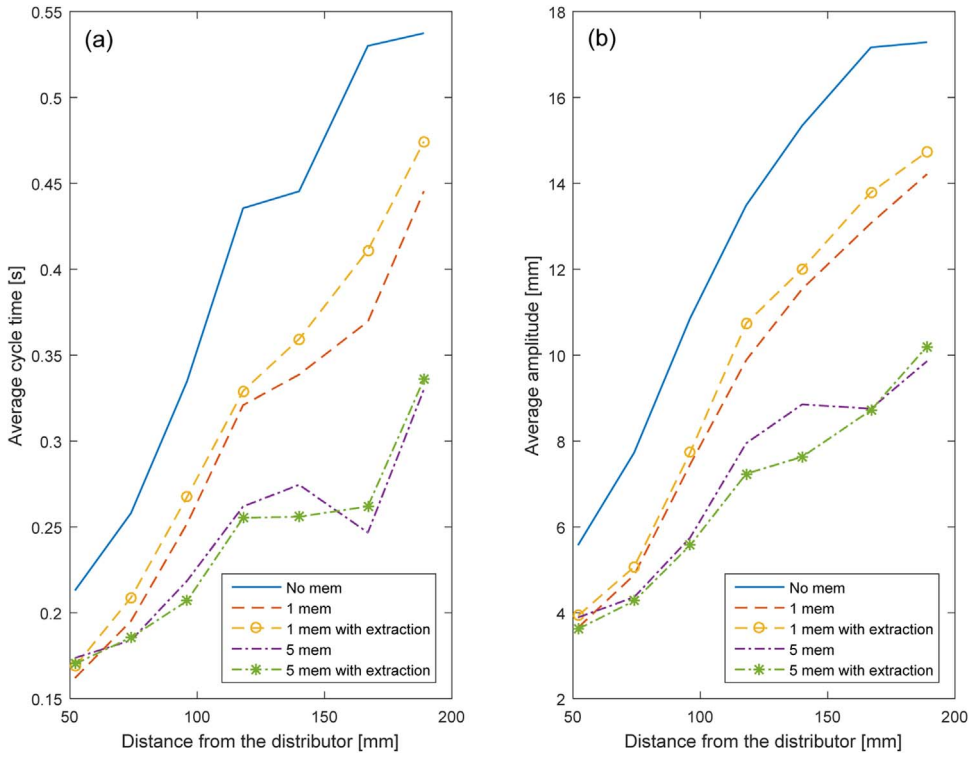

Fig. 14. (a) Average cycle time and (b) average amplitude of the output signal at different axial positions along the reactor (for all the cases the inlet velocity was corrected for membrane (s) presence and gas extraction to keep the outlet velocity at U/Umf = 2. Each point in the graphs represents the average of 2100 frames (at 35 Hz) over a pixel pocket of 50 × 50 at r/R = 0.5.

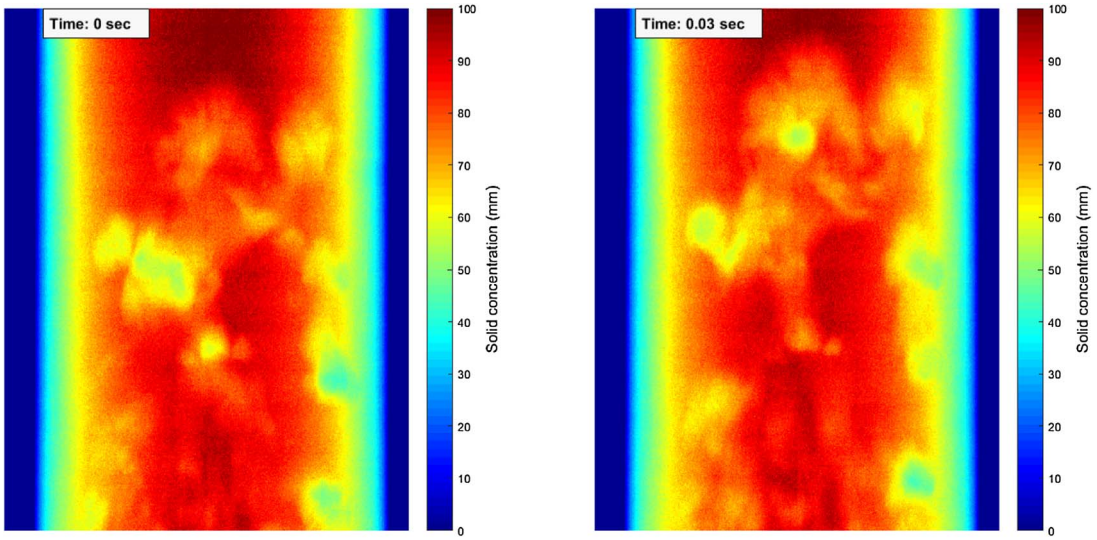

Fig. 15. Instantaneous solids concentration profiles at different moments in time for the standard bubbling fluidized bed without membranes at U/Umf = 2, where the bed was filled with fine Al2O3 particles (Geldart A/B), H = 80 mm.

inside the reactor, the average equivalent bubble diameter did not increase as much as for the single-membrane module, while the effect of the second spacer is more pronounced (Fig. 10b). At the second spacer the bubbles tend to pass more frequently close to the wall and later back again to the middle part of the reactor.

The lateral solids concentration profiles for the case of the module with one single membrane in the middle were plotted and compared at different distances from the bottom distributor plate and for the cases with and without membranes. Also the experimental results for the case with gas extraction (10 ln/min equal to 5% of inlet flow) was included. For all the cases the outlet velocity was kept at $U/U_{mf} = 2$ (the inlet flow rates were corrected for the reduced projected area of the membranes and for gas extraction).

Fig. 11a shows the obtained lateral solids concentration profiles for the case without immersed membranes at different axial distances from the distributor plate. For all the positions the average solids concentration decreases from the middle of the bed towards the reactor wall, as expected considering the relative small distance from the bottom distributor. Close to the reactor wall the solids concentration increases which is attributed to the solids back flow along the wall and the presence of the reactor wall. Moving from the bottom of the reactor to higher bed axial positions, the solids concentration decreases related to bubble growth; only when passing through the bottom spacer (63 mm above the distributor), the average solids concentration increases due to bubble cutting. Once more, this confirms the clear effect of the bottom spacer on the average bubble diameter.

When the membrane module with one single membrane was immersed inside the bed (Fig. 11b), the solids concentration was strongly increased near the membrane wall, even for the case without gas permeation through the membranes (due to a more frequent passage of gas bubbles inside the annular space of the reactor and far from the membrane). Thus it can be concluded that the formation of the so-called densified zones around the membrane(s) is not only due to gas extraction via the membranes, but also due to the presence of the membranes.

Inspecting Fig. 11c, no significant changes can be observed on the lateral solids concentration profiles related to the gas extraction (10 ln/min or 5% of the inlet flow), obviously related to the relatively small amount of gas extracted compared to the feed. To extend this study the experimental results from the case with the membrane module with five membranes (with and without gas extraction and up to 12.5% of the inlet flow rate) were analyzed (see Fig. 12).

As evident from Fig. 12a, and similar to the case with one single membrane submerged in the middle, higher average solids concentrations can be observed near the membranes. Moving from the reactor wall towards the middle of the reactor, the average solids concentration first increases to a maximum value and then decreases to a local minimum in the center of the reactor. This is related to the membrane module configuration, having five membranes located in a star shape without any membrane present in the middle of the module. Therefore, some bubbles will pass via the center of the module resulting in lower solids concentrations in the center.

Analyzing the effects of gas extraction via the membranes, the results for the case with gas extraction via the membranes (12.5 % of the inlet flow) showed no significant changes compared to the case without gas extraction in solids concentrations far from the bottom spacer (Fig. 12b). However, very close to the bottom spacer (i.e. at 70 mm distance from the distributor plate), the effect of gas extraction on the lateral solids concentration profiles is more pronounced, where higher solids concentrations were observed close to the membranes when extraction was imposed.

3.1.3. Bubble phase dynamics

In the previous section the average solids concentration was investigated for the cases with and without submerged membranes varying the number of membranes and the relative amount of gas extracted via the membranes. It was concluded that with the insertion of the membrane modules, higher solids concentrations was obtained along the reactor due to bubble cutting (reduced slug formation) when compared with the case without membranes present.

In order to substantiate this observation and to investigate the change in bubble phase behavior related to the presence of membranes, the average cycle time and the amplitude of the output signal at different bed positions can be used. Fig. 13 shows a typical output intensity signal over a pixel pocket of 50 × 50 pixels in size (at r/R = 0.5, where r is the radial distance from the center of the reactor and R is the reactor radius) averaged over 3 s of continuous recording for two cases at $U/U_{mf} = 0$ and at $U/U_{mf} = 2$. Inspecting the output signal for the case at $U/U_{mf} = 2$ (freely bubbling bed) reveals that the solids concentration is locally oscillating with an average amplitude and cycle time.

The oscillations in time of the solids concentration is attributed to the passage of bubbles. When a bubble passes, the solids concentration decreases to a minimum value (depending on the bubble size) and goes through a maximum when the bubble has just passed. For the case at $U/U_{mf} = 0$ (when the bed is stagnant), the standard deviation of the

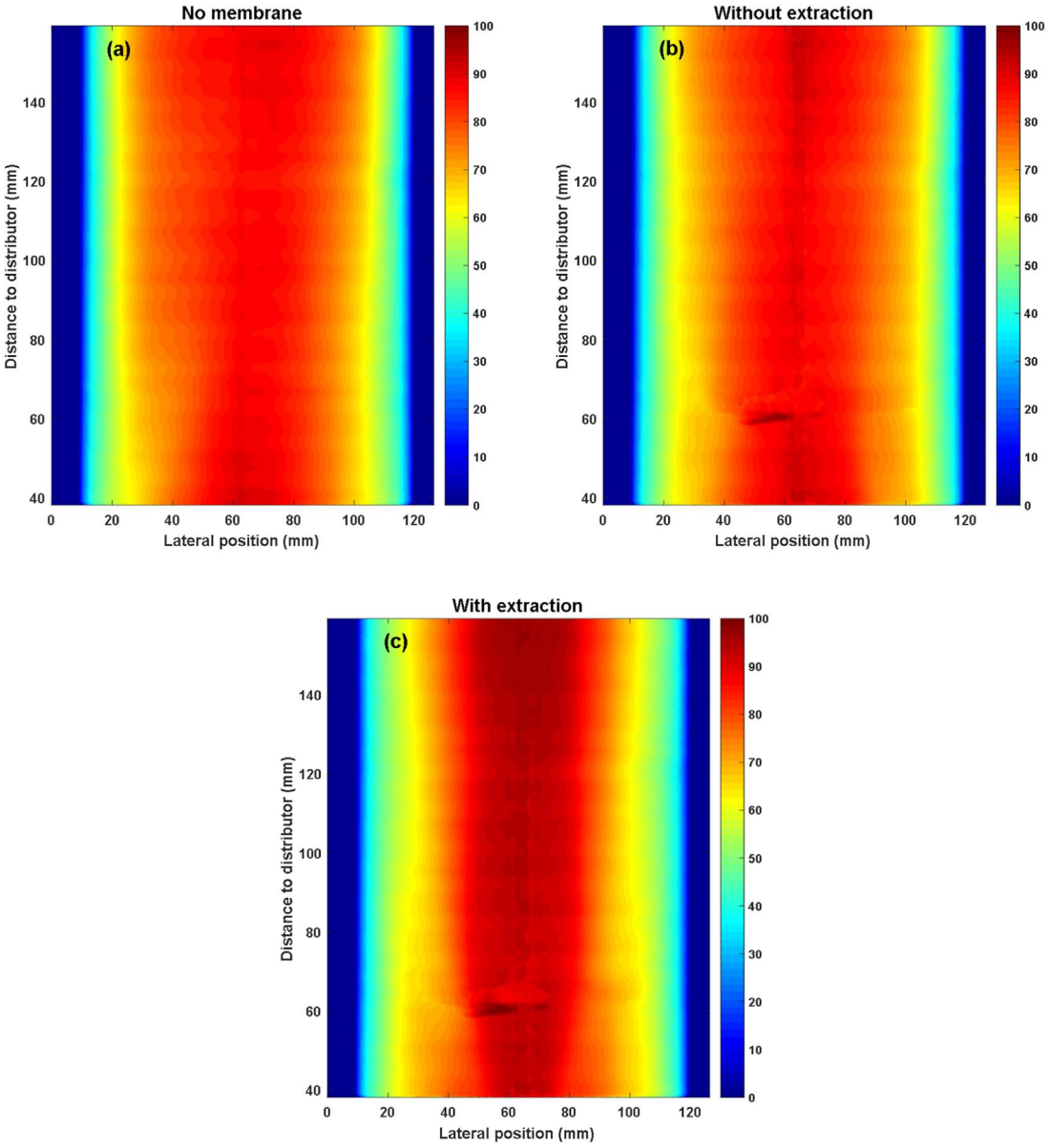

Fig. 16. Time-averaged solids concentration profiles for: (a) Standard fluidized bed without membranes; (b) Fluidized bed with one single membrane in the middle of the reactor without gas extraction; (c) Fluidized bed with one single membrane in the middle of the reactor and with 40% gas extraction (of the inlet flow). At H = 80 mm and U/U_{mf} = 2. The color bar represents the normalized solids concentration (path length) in mm of particles, where zero indicates the empty bed and 100 the packed bed.

output signal was 0.2357 (mean: 99 mm of solid), while for the case at U/U_{mf} = 2 the standard deviation increased to 13.88, confirming that the oscillations in solids concentrations is not caused by background noise (at U/U_{mf} = 0) and can be directly related to the passage of bubbles.

In order to quantify the bubble phase behavior at different experimental conditions, the output signal at the detector plate was monitored in time. Average cycle time and amplitude of the output signal was measured over 1 min of recording (2100 frames at 35 Hz) and at different axial positions along the reactor and in the middle of the annular space (r/R = 0.5). Three cases were selected for this analysis: 1) standard fluidized bed without internals; 2) Fluidized bed with one membrane in the middle without and with 10 ln/min gas extraction (5% of the inlet flow) through the membranes; 3) Fluidized bed with the membrane module consisting of five membranes without and with 25 ln/min gas extraction (12.5% of the inlet flow) via the membranes. Fig. 14 summarizes the obtained average cycle time and amplitudes for all these cases.

Fig. 14a shows that for the case without membranes, at higher axial positions from the distributor plate, a higher average cycle time is measured. This is expected due to bubble growth along the reactor length. The same trend can be seen for the average amplitude at different axial positions (Fig. 14b). This confirms the fact that at higher bed positions the bubble phase will grow to bigger bubbles that occupy a larger bed depth. In the presence of one single membrane in the middle of the reactor, the average output signal cycle time was reduced by 24% along the reactor (28% reduction in signal amplitude) in comparison with the case without immersed membranes. For the same case with gas extraction (5% of the inlet) the average cycle time was decreased by 20% compared to the case without membranes.

When the membrane module with 5 membranes was immersed inside the bed (no extraction), the reduction in the average output signal cycle time was 36%, while the average signal amplitude was reduced by 42%. This confirms that when a higher number of membranes are submerged, a higher degree of bubble cutting can be obtained. When 12.5% of the inlet gas was extracted via the membranes no significant changes in the average signal properties were observed (37% reduction in average cycle time and 45% reduction in amplitude

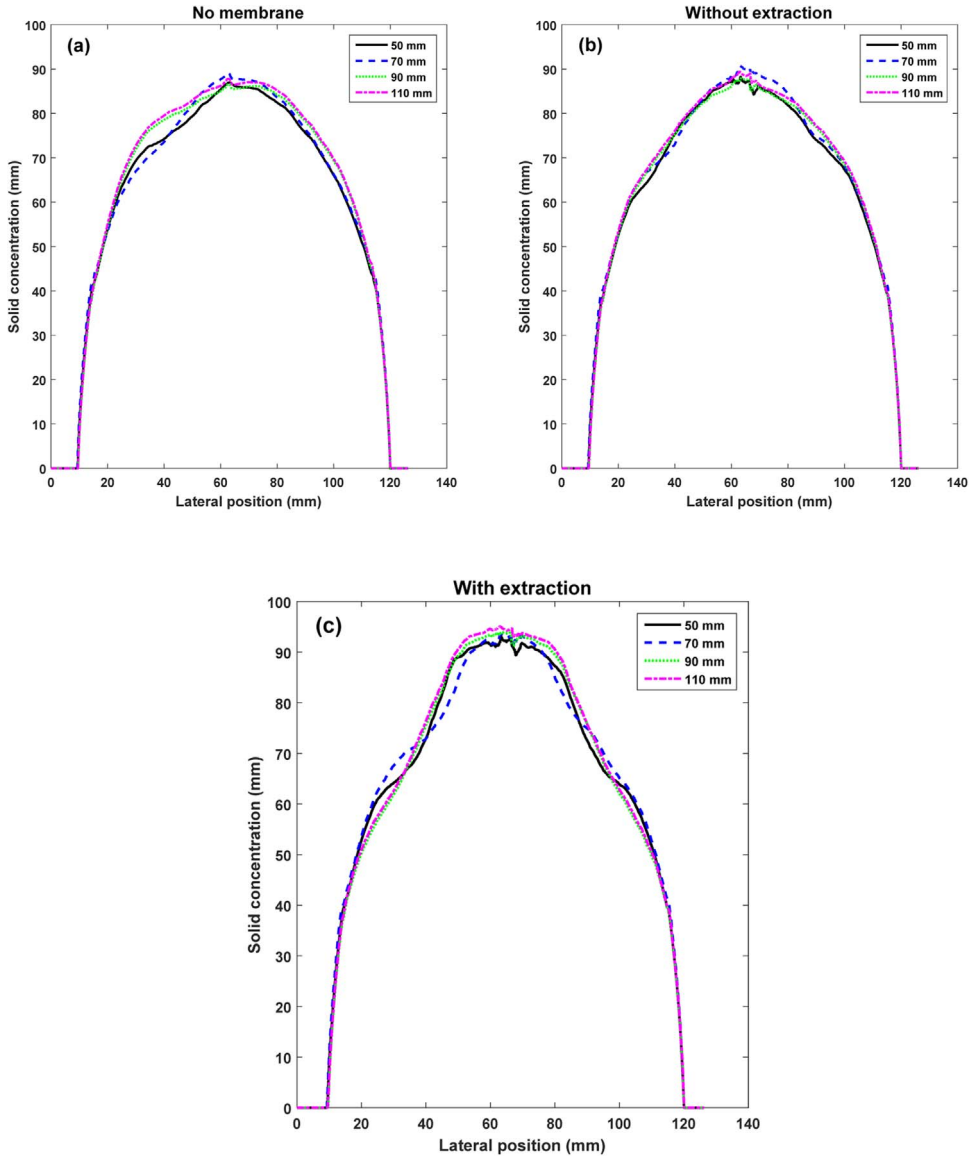

Fig. 17. Average lateral solids concentration profiles at different distances from the distributor plate: (a) Standard fluidized bed without membrane (b) Fluidized bed with one single membrane in the middle without gas extraction (c) Fluidized bed with one single membrane in the middle with 40% gas extraction (of the inlet flow). For all the cases the outlet velocity was kept at $U/U_{mf} = 2$.

compared with the case without membranes). In general, with submerged membranes a lower amplitude and cycle time was observed along the reactor length, with a more pronounced effect for the module with more membranes.

3.2. Geldart A/B

After the experiments with the polystyrene particles and at different operating conditions, the reactor was refilled with fine Al_2O_3 particles (Geldart A/B type). The stagnant bed height was 30 cm giving a bed aspect ratio of 3. Thus, it was ensured that the membrane module was fully immersed at minimum fluidization conditions. The lower minimum fluidization velocity for this type of particles required a lower inlet flow rate, allowing to achieve much higher values of gas extraction (up to 40% of the inlet flow).

Fig. 15 shows the instantaneous solids concentration profiles from the experiment at $U/U_{mf} = 2$ for the case without membranes. Compared to a similar case with Geldart B type particles at the same fluidization number and at the same height from the distributor plate, a clearly larger and more homogeneous average solids concentration was observed, without slug formation.

The results shown in Fig. 15 also imply that for fluidized bed reactors designed especially for micro heat and power applications (with similar reactor sizing as the fluidized bed used in this study), a smaller average bubble diameter without slug formation can be obtained when using Geldart A/B type particles, with an expected positive effect on the bubble-to-emulsion phase mass transfer rate. In the next section the effect of the presence of and the permeation through a submerged membrane is investigated on the average solids concentration profiles.

3.2.1. Average solids concentration

The measured time-averaged solids concentration profiles for three different cases have been presented in Fig. 16a) standard fluidized bed without membranes; b) Fluidized bed with one single membrane in the middle and without gas extraction and c) Fluidized bed with one single membrane in the middle of the reactor and 40% gas extraction (of the inlet flow). For all the cases the highest average solids concentration was found in the middle of the reactor. Note that these time-averaged solids concentrations are much higher than the solids concentrations

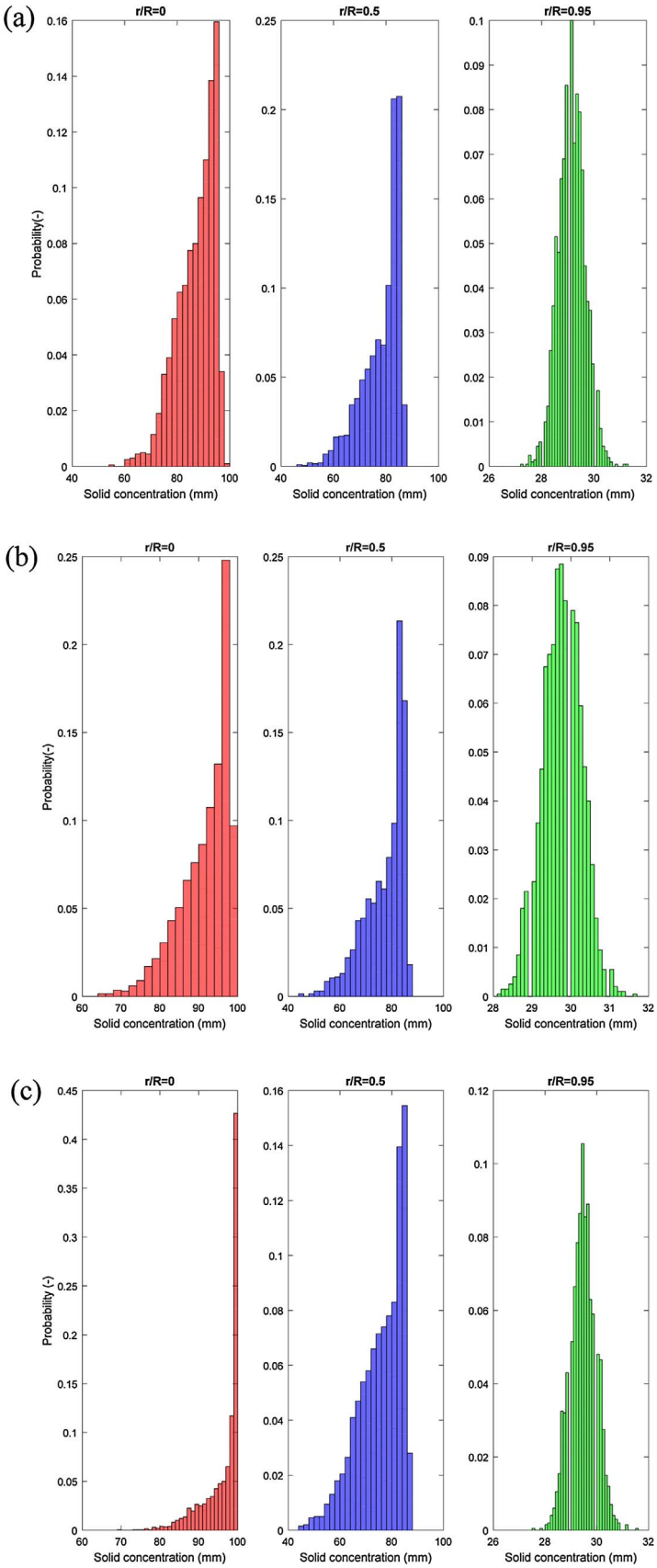

Fig. 18. Normalized histograms at different lateral positions across the reactor width and for three different cases: (a) Standard fluidized bed without membrane; (b) Fluidized bed with one single membrane immersed in the middle of the reactor without gas extraction; (c) Fluidized bed with one single membrane in the middle of the reactor with 40% gas extraction (of the inlet flow). For all the cases the outlet velocity was kept the same at $U/U_{mf} = 2$.

measured for the polystyrene particles (Geldart B) at the same relative fluidization velocities, related to the smoother fluidization with smaller average bubble sizes.

When a membrane module with one single membrane was integrated inside the bed (Fig. 16b), the average solids concentration was slightly decreased in the annular space between the membrane and the reactor wall, indicating that more bubbles pass between the membrane and reactor wall while far from the membrane and at the reactor wall no significant changes can be discerned.

In the presence of the membrane with gas extraction (40% of the inlet flow), a more clear change in the average solids concentrations was observed (Fig. 16c). Especially near the surface of the membrane the average solids concentration shows a layer with maximum solids concentration. Far from the membrane surface and in the middle of the annular space (r/R = 0.5), a lower solids concentration was detected compared to the case without gas extraction. These results confirm that at sufficiently high extraction values, particles will accumulate near the membrane surface and form a densified layer which may impose an additional mass transfer resistance for gas components to reach the surface of the membranes [13]. Fig. 17 shows the time-averaged lateral solids concentration profiles at different distances from the distributor plate and for the three different cases, supporting the above observations.

To investigate whether the densified solids layer near the membrane is stagnant or dynamic, the temporal evolution of the solids concentration was monitored at three different radial positions: 1) At the surface of the membrane at r/R = 0; 2) In the middle of the annular space at r/R = 0.5 and 3) Next to the reactor wall at r/R = 0.95 (all the points were located at 10 cm from the bottom distributor plate). For each case the solids concentration was measured and saved over 2100 frames (one minute of recording with 35 frames per second) and the histogram of the obtained solids concentration data, normalized by the total number of observations in each histogram bin, is given in Fig. 18.

3.2.2. Solids probability distribution

The probability distribution of the solids concentrations in the center of the column (r/R = 0) show for all the three different cases a skewness towards high solids concentrations, which increases due to the presence of the membrane and even more in case of gas extraction through the membrane. In case of gas extraction via the membrane in the center of the bed (Fig. 18c), over 40% of the incidents the solids concentration reached the maximum value of 100 mm of bed depth, corresponding to the maximum packing of a packed bed, implying that for over 40% of the incidents no bubbles were passing near the membrane surface. Moving away from the surface of the membrane to the middle of the annular space (r/R = 0.5), the immersion of the membrane results in higher probabilities for lower solids concentrations compared with the case without membrane in the bed. This confirms that the immersion of the membrane results in a higher gas bubble passage in the annular space. At the reactor wall (r/R = 0.95) a more Gaussian probability distribution can be observed for all the three scenarios. At the reactor wall no significant changes were observed when the membrane module was immersed inside the bed, or when 40% of the gas was extracted via the membrane.

4. Conclusions

The hydrodynamics of a 10 cm diameter membrane-assisted fluidized bed was investigated using a fast X-ray analysis technique. For each experiment the output attenuation of the X-ray beam was measured at the detector plate for over one minute of continuous recording. A total number of 2100 frames (at 35 Hz) was saved for all experiements. The projected 2D solids concentration maps were obtained after a detailed image correction and calibration procedure.

Two different membrane modules with one and five membranes were designed and constructed to monitor the behavior of the fluidized bed in absence and in presence of the membrane modules and with and without gas extraction through the membranes. Two different particle types were investigated, viz. 400–600 μm polystyrene and 80–200 μm Al_2O_3 particles, belonging to type B and A/B of the Geldart classification, respectively.

The obtained results revealed the heavy slugs formation when using the Geldart B type particles without the membrane modules. The formation of these slugs corresponds with a strong decrease in the time-averaged solids concentrations inside the fluidized bed and may increase the overall mass transfer resistance and increase gas bypass, thus possibly deteriorating the reactor performance. Once the membrane modules were immersed inside the fluidized bed, the extent of slugging was largely decreased attributed to increased bubble breakage.

At higher axial positions inside the fluidized bed, the average bubble diameter increased, which may impose or aggravate mass transfer limitations between the bubble and emulsion phases. In a research study by Gallucci et al. [24] it was proposed to circumvent these mass transfer limitations by using spacers (e.g. wire mesh) inside the bed. Results from our study indicated that the membrane modules (membranes/spacers) can be used not only to extract (and purify) gas from the reactor, but can simultaneously be exploited to limit bubble growth along the reactor height.

Placing the membrane spacers far from each other resulted in reduced bubble cutting along the bed. Decreasing the distance between the spacers (shorter membranes) may also be beneficial to keep the membranes better fixed and improve their lifetime depending on the membranes' mechanical stability. Thus, positioning more spacers with shorter membranes may improve both the hydrodynamics and the mechanical stability of the membranes. This will result in a smaller average bubble diameter and enhanced mass transfer between emulsion and bubble phases.

The obtained results for the time-averaged solids concentration fields for the case of the membrane module with one membrane in the center and using Geldart A/B type particles confirmed that at high extraction values, particles will accumulate near by the membrane and form a layer which may induce an additional mass transfer resistance for gas components to reach the surface of the membranes, whereas more bubbles were passing in the annular space between the membrane and the reactor wall. This was further supported by the probability density function of the solids concentration at different radial positions. The results from this study can help optimizing the positioning of the membrane and membrane spacers for optimal performance of fluidized bed membrane reactors.

References

[1] G. Di Marcoberardino, L. Roses, G. Manzolini, Technical assessment of a micro-cogeneration system based on polymer electrolyte membrane fuel cell and fluidized bed autothermal reformer, Appl. Energy 162 (2016) 231–244, http://dx.doi.org/10.1016/j.apenergy.2015.10.068.

[2] A. Brunetti, E. Drioli, G. Barbieri, Energy and mass intensities in hydrogen upgrading by a membrane reactor, Fuel Process. Technol. 118 (2014) 278–286, http://dx.doi.org/10.1016/j.fuproc.2013.09.009.

[3] F. Gallucci, E. Fernandez, P. Corengia, M. van Sint Annaland, Recent advances on membranes and membrane reactors for hydrogen production, Chem. Eng. Sci. 92 (2013) 40–66, http://dx.doi.org/10.1016/j.ces.2013.01.008.

[4] A. Helmi, E. Fernandez, J. Melendez, D.A. Pacheco Tanaka, F. Gallucci, M. van Sint Annaland, Fluidized bed membrane reactors for ultra pure H_2 production-a step forward towards commercialization, Molecules 21 (2016), http://dx.doi.org/10.3390/molecules21030376.

[5] E. Fernandez, J.A. Medrano, J. Melendez, M. Parco, J.L. Viviente, M. van Sint Annaland, F. Gallucci, D.A. Pacheco Tanaka, Preparation and characterization of metallic supported thin Pd-Ag membranes for hydrogen separation, Chem. Eng. J. 305 (2016) 182–190, http://dx.doi.org/10.1016/j.cej.2015.09.119.

[6] E. Fernandez, A. Helmi, K. Coenen, J. Melendez, J.L. Viviente, D.A. Pacheco Tanaka, M. van Sint Annaland, F. Gallucci, Development of thin Pd-Ag supported membranes for fluidized bed membrane reactors including WGS related gases, Int. J. Hydrogen Energy 40 (2015) 3506–3519, http://dx.doi.org/10.1016/j.ijhydene.2014.08.074.

[7] E. Fernandez, J. Angel Sanchez-García, J. Melendez, V. Spallina, M. van Sint Annaland, F. Gallucci, D.A. Pacheco Tanaka, Development of highly permeable

ultra-thin Pd-based supported membranes, Chem. Eng. J. 305 (2016) 149–155, http://dx.doi.org/10.1016/j.cej.2015.11.060.
[8] T.A. Peters, M. Stange, R. Bredesen, On the high pressure performance of thin supported PdAg membranes – evidence of ultra high hydrogen flux after air treatment, J. Membr. Sci. 378 (1–2) (2011) 28–34.
[9] T.A. Peters, T. Kaleta, M. Stange, R. Bredesen, Hydrogen transport through a selection of thin Pd-alloy membranes: membrane stability, H_2S inhibition, and flux recovery in hydrogen and simulated WGS mixtures, Catal. Today 193 (2012) 8–19, http://dx.doi.org/10.1016/j.cattod.2011.12.028.
[10] J.F. De Jong, M. van Sint Annaland, J.A.M. Kuipers, Experimental study on the hydrodynamic effects of gas permeation through horizontal membrane tubes in fluidized beds, Powder Technol. 241 (2013) 74–84, http://dx.doi.org/10.1016/j.powtec.2013.03.014.
[11] J.A. Medrano, R.J.W. Voncken, I. Roghair, F. Gallucci, M. van Sint Annaland, On the effect of gas pockets surrounding membranes in fluidized bed membrane reactors: an experimental and numerical study, Chem. Eng. J. 282 (2015) 45–57, http://dx.doi.org/10.1016/j.cej.2015.04.007.
[12] N.T.Y. Dang, F. Gallucci, M. van Sint Annaland, Micro-structured fluidized bed membrane reactors: solids circulation and densified zones distribution, Chem. Eng. J. 239 (2014) 42–52, http://dx.doi.org/10.1016/j.cej.2013.11.001.
[13] L. Tan, I. Roghair, M. van Sint Annaland, Simulation study on the effect of gas permeation on the hydrodynamic characteristics of membrane-assisted micro fluidized beds, Appl. Math. Model. 38 (2014) 4291–4307, http://dx.doi.org/10.1016/j.apm.2014.04.044.
[14] S.A. Wassie, F. Gallucci, S. Cloete, A. Zaabout, M. van Sint Annaland, S. Amini, The effect of gas permeation through vertical membranes on chemical switching reforming (CSR) reactor performance, Int. J. Hydrogen Energy 41 (2015) 8640–8655, http://dx.doi.org/10.1016/j.ijhydene.2015.12.003.
[15] S. Maurer, E.C. Wagner, T.J. Schildhauer, J.R. van Ommen, S.M.A. Biollaz, R.F. Mudde, X-ray measurements of bubble hold-up in fluidized beds with and without vertical internals, Int. J. Multiph. Flow 74 (2015) 118–124, http://dx.doi.org/10.1016/j.ijmultiphaseflow.2015.03.009.
[16] S. Maurer, E.C. Wagner, J.R. van Ommen, T.J. Schildhauer, S.L. Teske, S.M.A. Biollaz, A. Wokaun, R.F. Mudde, Influence of vertical internals on a bubbling fluidized bed characterized by X-ray tomography, Int. J. Multiph. Flow 75 (2015) 237–249, http://dx.doi.org/10.1016/j.ijmultiphaseflow.2015.06.001.
[17] S. Maurer, D. Gschwend, E.C. Wagner, T.J. Schildhauer, J.R. van Ommen, S.M.A. Biollaz, R.F. Mudde, Correlating bubble size and velocity distribution in bubbling fluidized bed based on X-ray tomography, Chem. Eng. J. 298 (2016) 17–25, http://dx.doi.org/10.1016/j.cej.2016.02.012.
[18] R.F. Mudde, Bubbles in a fluidized bed: a fast X-ray scanner, AIChE J. 57 (2011) 2685–2690, http://dx.doi.org/10.1002/aic.
[19] R.F. Mudde, J. Alles, T.H.J.J. van der Hagen, Feasibility study of a time-resolving x-ray tomographic system, Meas. Sci. Technol. 19 (2008) 85501, http://dx.doi.org/10.1088/0957-0233/19/8/085501.
[20] RE4CELL, Advanced Multi-Fuel Reformer for Fuel CELL CHP Systems − ReforCELL, (n.d.). http://www.reforcell.eu/ (Accessed August 8, 2016).
[21] E. Fernandez, J. Sanchez-Garcia, J. Viviente, M. van Sint Annaland, F. Gallucci, D.A. Pacheco Tanaka, Morphology and N_2 permeance of sputtered Pd-Ag ultra-thin film membranes, Molecules 21 (2016) 210, http://dx.doi.org/10.3390/molecules21020210.
[22] DEMCAMER, Design and manufacturing of catalitic membranes reactors by developing new nano-architectured catalytic and selective membrane materials, (n.d.). http://demcamer.org/ (Accessed August 8, 2016).
[23] D. Geldart, Types of gas fluidization, Powder Technol. 7 (1973) 285–292, http://dx.doi.org/10.1016/0032-5910(73)80037-3.
[24] F. Gallucci, M. van Sintannaland, J.A.M. Kuipers, Theoretical comparison of packed bed and fluidized bed membrane reactors for methane reforming, Int. J. Hydrogen Energy 35 (2010) 7142–7150, http://dx.doi.org/10.1016/j.ijhydene.2010.02.050.